RSC Advances

ROYAL SOCIETY OF CHEMISTRY

www.rsc.org/advances

Polybenzimidazole and Polybenzimidazole/MoS_2 Hybrids as an Active Nitrogen Sites: Hydrogen Generation Application

Mohammad Dinari [1], Afshin Nabiyan [1], Ali. A. Ensafi [1], Mehdi Jafari-Asl [1]

[1]Department of Chemistry, Isfahan University of Technology, Isfahan 84156–83111, Islamic Republic of Iran

Abstract: Development free metals or non-noble-metal catalysts for electrode materials with both excellent activity and high stability is essential for hydrogen production. In this work, high rich nitrogen polybenzimidazole (PBI) networks was synthesized through a one-step polycondensation of 1,2,4,5-tetraaminobenzene with 4,4',4''-((1,3,5-triazine-2,4,6-triyl)tris(azanediyl))tribenzoic acid. Then, organic/inorganic nanohybrids of PBI with amorphous MoS_2 nanoplates (PBI-MoS_2) were prepared. The structural characterization and morphological of these novel hybrids were studies using FT-IR, ^{1}H NMR, elemental analysis, thermogravimetry, transmission electron microscopy, field-emission scanning electron microscopy and X-ray diffraction techniques. Electrochemical studies revealed the onset potential of only (–160 mV vs. RHE) with a small Tafel slope of 50.6 mV dec^{-1} for hydrogen generation reaction in 0.5 mol L^{-1} H_2SO_4. Stability tests through long term potential cycles confirm the excellent durability of PBI-MoS_2 in acid media. The outstanding hydrogen generation activity is derived from the electronic penetration effect and H^+ absorption of pyridinic-N and/or pyrrolic-N as active sites at per repeat of the PBI matrix. It is worth noting

[1] - Corresponding author. Tel.: +98 3133913270; fax: +98 3133912351.

E-mail address: dinari@cc.iut.ac.ir; mdinary@gmail.com

that pure PBI and PBI-MoS_2 hybrids, for the first time, were used as both anode and cathode in two-electrode system open up new possibilities for exploring overall hydrogen generation technology catalysts in acidic electrolyte. This development offers an attractive electrocatalyst for large-scale hydrogen generation.

Keywords: Hydrogen generation; Polybenzimidazole; pyridinic-N; Pyrrolic-N molybdenum disulfide.

1. Introduction

The rapid growth of global energy consumption and the associated environmental issues have triggered the urgent demand for renewable and clean energy sources. Electrochemical water splitting driven by solar energy has been considered as an attractive approach to produce hydrogen (H_2) fuel, a sustainable, secure and environmentally benign energy vector. Efficient water splitting requires high-performance electrocatalysts to promote the hydrogen generation reaction.[1-3] The catalysts are cornerstone of this type of reaction.[4] There is now enormous interest to design and develop efficient and inexpensive catalysts to generate hydrogen.[5] According to the information, which provided by the previous reports only a few synthetic catalysts are known to operate in water and they were able to give a high current density at a low overpotential (Ƞ).[6-9] To date, the most effective hydrogen generation catalyst are Pt group metals, whose huge scale application has been severely limited by their low abundance and high cost.[7-10] Therefore, finding an inexpensive catalyst still is a serious challenge for hydrogen generation. In earlier works, scientific researches in catalyst areas achieve new approaches, which are used from metal-free catalysts for hydrogen generation such as 4,4′-bipyridine, nitrogen doped reduce graphene oxide, metal-free polymeric photocatalyst, and etc.[11-13] A large proportion of metal-free catalysts like 4,4′-bipyridine and

of nitrogen doped reduces graphene oxide, the pivotal role of the nitrogen element is inevitable and it has crucial junction in most catalyst mechanism of hydrogen generation reaction. Therefore, a metal-free catalyst that is able to incorporate by nitrogen with hydrogen generation mechanism like Volmer, Tafel or Heyrovsky reaction is among the most outstanding catalyst for hydrogen generation.[11]

Polybenzimidazole (PBI) PBI is a basic polymer with good thermal and chemical stability, which belongs to the class of heterocyclic polymers that contain benzimidazole units.[14] PBI is the most promising candidate polymer to use as a hydrogen generation catalyst. There have been a numerous reasons why PBI consider or offer as a catalyst in hydrogen generation reaction and it would explore only a few most important properties for hydrogen generation once here. First of all, PBI has considerable proton conductivity as long as doped or hybrid with conductive materials such as graphene and phosphoric acid.[15,16] In some studies, the enhanced electrocatalytic activity of hydrogen generation catalyst is attributed to pyridinic-N and/or pyrrolic-N. Therefore, PBI which is used as a membrane materials for fuel cells, can repeat the pyridinic-N and/or pyrrolic-N in every per repeat unit.[13,17-19] PBI show high surface areas with porous materials to enhance fast mass transport of reagents. Therefore, the high surface area is able to accept PBI as eligible catalyst.[20-22] This vital information can be confirmed that PBI as is a good catalyst candidate for hydrogen generation.

In the past years, organic/inorganic hybrid nanocomposites (NCs) as long as the organic part is the polymer matrix and the inorganic part is nanosized fillers have been advanced widely since their specific properties and particular application of NCs achieve after hybridization.[23-25] Polymer/layered inorganic NCs have attracted great consideration for their potential in improving polymer properties such as mechanical, thermal, and physical properties.[23-25] Molybdenum disulfide (MoS_2) nanosheets are expected to become one kind of

useful fillers for improving the properties of polymers.[26] MoS_2 has attracted considerable interest over the last few years due to its extraordinary optical, thermal, and mechanical properties arising from its exceptional structure.[27,28] The unique sandwich structure has potential applications in many technological fields, such as super lubricant, sensors, batteries, photocatalyst, hydrogen storage and NCs.[29-31] where MoS_2-based polymer composites are a novel class of materials that combine the attractive functional properties of MoS_2 (electrical, optical, thermal, mechanical properties, etc) with the advantages of polymers, such as low cost and good processability.[32]

Motivated by these results, in this work, we sought to explore a facile and efficient route for preparing PBI/MoS_2 NCs. First, 4,4',4"-((1,3,5-triazine-2,4,6-triyl) tris (azanediyl)) tribenzoic acid (TCA) was prepared from reaction between cyanuric chloride and para-aminobenzoic acid in glacial acetic acid. Then, PBI networks was synthesized through a facile one step polycondensation reaction of 1,2,4,5-tetraaminobenzene and TCA using methane sulfonic acid and phosphorus pentoxide mixture as a reaction medium. MoS_2 plate was synthesized by hydrothermal method and the PBI-MoS_2 NCs was achieved by ultrasonic irradiation methods. Although there are numerous reports in the literature for MoS_2 as electrocatalyst for hydrogen generation, to the best of our knowledge, there is no report which addresses PBI as well as PBI-MoS_2 hybrid as hydrogen generation electrocatalysts. The electrocatalytic analysis results such as onset potentials, Tafel slopes and current densities exhibited infinitely superior and favorable catalytic activities of PBI and PBI-MoS_2 hybrids electrocatalyst for hydrogen generation.

2. Experimental

2.1. Reagents

Cyanuric chloride, methanesulfonic acid, and phosphorus pentoxide were purchased from Merck chemical Co. and 1,2,4,5-benzenetetramine tetrahydrochloride, L-cysteine,

Nafion solution (5.0 wt. % in lower aliphatic alcohols and water), 4-aminobenzoic acid and ammonium molybdate tetrahydrate, ($(NH_4)_6Mo_7O_{24}$. $4H_2O$) were purchased from Sigma Aldrich. All other chemicals used in this investigation were of analytical grade and were purchased from Merck. Deionization water (DI) was used for preparation of all of solution.

2.2. Instrumentation

Fourier-Transform Infrared (FT-IR) spectrums of the materials were recorded using a JASCO 680 (Japan) spectrophotometer over the wavenumber range of 400–4000 cm^{-1}. ^1H NMR spectra was recorded on Bruker Avance 400 MHz spectrometer operating on polymer solution in dimethyl sulfoxide-d6 (DMSO-d6). Chemical shifts are given in the δ scale in parts per million (ppm). Thermal properties of the compounds was performed with a STA503 win TA (Bahr-Thermoanalyse GmbH, Hüllhorst, Germany) at a heating rate of 10 ^oC/min from 25 to 800 °C under nitrogen atmosphere. The composition of the polymer (C, H, and N) was analyzed by elemental analysis (LECO, CHNS-932). The X-ray diffraction (XRD) was used to characterize the crystalline structure of the polymer and NCs. XRD patterns were collected on a Bruker, D8ADVANCE (Germany). Transmission electron microscopy (TEM) was performed using a Philips CM120. Morphology was observed using field-emission scanning electron microscopy (FE-SEM, MIRA FE-SEM | TESCAN, Mira 3-XMU).

2.3. Electrochemical characterizations

The electrochemical measurements were performed in 0.5 mol L^{-1} H_2SO_4 solution at room temperature (RT). The electrode potential was controlled by an Autolab electrochemical analyzer, Model PGSTAT 30 potentiostat /galvanostat (Eco-Chemie, The Netherlands). Data were acquired and processed (background correction) using the GPSE and FARA computrace software 4.9.007. A standard three-electrode cell containing a platinum wire auxiliary electrode, a saturated Ag/AgCl reference electrode and PBI/MoS_2 and/or PBI modified glasy carbon electrode as a working electrode.

2.4. Preparation of the working electrodes

The glassy carbon electrode (GCE) was polished to a mirror finish using alumina powder. After that, the electrode was washed several times with DI water and ethanol. Then, 10 mL of catalyst ink (PBI/MoS_2 and PBI, that prepared by dispersing of 2.5 mg of the as prepared catalysts in 1 mL of ethanol/water (1:1)) was drop-coated on the polished GCE electrode surface. After drying, 5 mL of 5.0 wt. % Nafion solution in lower aliphatic alcohols and water was coated on the catalyst layer to ensure better adhesion of the catalyst on the glassy carbon substrate. This electrode was then dried under room temperature.

2.5. Preparation of 4,4',4''-((1,3,5-triazine-2,4,6-triyl)tris(azanediyl))tribenzoic acid

4,4',4''-((1,3,5-triazine-2,4,6-triyl) tris(azanediyl))tribenzoic acid (TCA) as a three acid monomer was prepared according to the reported procedure.[33] Briefly, cyanuric chloride (3.68 g, 20 mmol) was added in one portion to a stirred solution of a 4-aminobenzoic acid (33 mmol) in 150 mL of glacial acetic acid and the mixture was refluxed for 12 h. The products were precipitated from the mixture as white solids and were recovered by filtration. The solid products were washed with boiling water to neutral pH and dried at 90°C in air.

2.6. Preparation of star polybenzimidazole

Star PBI was synthesized by polycondensation method. In a typical procedure, a three-necked flask equipped with a mechanical stirrer and N_2 inlet, was charged with 3.0 g of phosphorus pentoxide and 20 mL of methanesulfonic acid. The mixture was stirred at 50 ^oC under a nitrogen flow until phosphorus pentoxide dissolved. Then, TCA (0.69 g) and 1,2,4,5-tetraaminobenzene (0.29 g) were added and the temperature was increased and the mixture was allowed to polymerize at 80 ^oC for 2 h, 100 ^oC for 1 h, 120 ^oC for 1 h ,and 140 ^oC for 3 h. The resulting mixture was poured into ice water and then collected by filtration. The solid was washed with ammonia solution and then with deionized water to neutrality and remove

the possibly unreacted monomers. Final, the perception was dried at 100 ^{o}C under vacuum to constant weight. Yield: 90%.

2.7. Preparation of molybdenum disulfide

MoS_2 was synthesized according to the reported procedure.[34] Briefly, 1.5 mmol of $((NH_4)_6Mo_7O_{24}\,4H_2O$ was dissolved in 30 ml deionized water, and then a given amount of L-cysteine was added into the solution under violent stirring. After stirring for 10 min, approximately, 12 mol/L HCl was added into the above solution mixture drop by drop under stirring to adjust the pH value to less than 1. Finally, the solution was transferred into a 100 ml Teflon-lined stainless steel autoclave and heated at 240 °C for 24 h. After cooled to room temperature naturally, the black precipitates of MoS_2 were collected, washed with distilled water and absolute ethanol for several times, and then dried in vacuum at 60 °C for 12 h.

2.8. Preparation of polybenzimidazole/molybdenum disulfide (PBI/MoS_2) hybrids

For preparations of PBI-MoS_2 hybrid, 0.1 g of the PBI was dispersed in 10 mL of DMSO and a uniform colloidal dispersion was obtained after sonication for 2h at room temperature. Then the suspension was mixed with the different amounts of MoS_2 (1, 5 and 10%wt) to produced electrocatalyst followed by sonication for 2 h and stirred for 3 day at 110 ^{o}C. The solvent was removed and the powders obtained were dried under vacuum for 24 h at 60 ^{o}C. The NCs are named as PBI/MoS_2 NC1%, PBI/MoS_2 NC5% and PBI/MoS_2 NC10%, where the percentage given in the genetic abbreviations is the weight percentage.

3. Results and discussion

3.1 Synthesis, structural characterization and morphological investigation

The synthesis of the triazine based monomer is presented in Fig 1. TCA was prepared through a successive procedure of aryl amination of cyanuric chloride with para-aminobenzoic acid in glacial acetic acid. The synthesis route to polybenzimidazole networks

is outlined in Fig. 1. PBI was respectively prepared by TCA and 1,2,4,5-tetraaminobenzene *via* a one-step polycondensation in a solution of phosphorus pentoxide in methanesulfonic acid *i.e*. Eaton's reagent. Eaton's reagent has been reported for the preparation of linear PBIs, and it has been found that the polymerization system has, a high reaction temperature and a low viscosity, less reaction time and high catalytic efficiency.[35] To clarify, it was observed here that the target polymerizations proceeded clearly and could be completed within several hours at a temperature below 140 ^{o}C. The obtained light brown products are insoluble in many common solvents. **"Figure 1 Here"**

Fig.2 shows FTIR spectra of the triazine based monomer (TCA), MoS_2, neat PBI and PBI NCs with different amount of MoS_2. For TCA monomer, the FTIR spectrum shows the broad bond around 2600-3500 cm^{-1} for acid functional groups. Absorbance of the NH group was appeared around 3550 cm^{-1}. Peaks correspond to C=N in cyanuric ring is shown at 1500-1600 cm^{-1}. Also, the carbonyl groups of TCA appeared around 1706 cm^{-1} (Fig. 2a). After polymerization of TCA with tetraamine monomer, new absorbance bond corresponded to the PBI was appearing and broad bond in the range of 2600-3500 cm^{-1} was disappeared to confirm the formation of the polymer (Fig. 2b). The board band from 3450 to 3400 cm^{-1} is attributed to the isolated N-H stretching of the imidazole, whereas the broad band near 3250-2900 cm^{-1} is assigned to the self-associated N-H bond. This band is broader in the presence of moisture (-OH). The C=C and C=N stretching appear in the region of 1630-1500 cm^{-1}. A strong band at 1400-1390 cm^{-1} must be attributed to the deformation of benzimidazole rings and inplane C-H deformations appear at 1235-1225 cm^{-1} in PBI.[36,37] Moreover, it is clear that the FTIR spectrum of PBI/MoS_2 NCs shows the same characteristic signals with pure PBI. All characteristic peaks related to the PBI such as NH, C=N, C=C, C-N, C-C and C-H were appearing in the FTIR spectra of the NC materials. The FTIR results indicate that PBI/MoS_2 NCs have been prepared successfully. **"Figure 2 Here"**

The formation of PBI polymer was confirmed by the ^{1}H NMR spectra as shown in Fig. 3. In this Fig., the peak of the imidazole proton was observed at 12.74 ppm, and secondary amine (aromatic N-H) was observed at 9.75 ppm as well as all of the aromatic protons were appeared at 7-9 ppm and confirmed the formation of the PBI.[38]

"Figure 3 Here

The composition of the C, H, and N in the PBI structure was analyzed by elemental analysis, as shown in Table 1. It is known that PBI is very hygroscopic. During the sample preparation and handling for elemental analysis, the PBI absorbed water from air. The residual percentage due to the oxygen element in the structure is caused by absorbed water throughout the analysis. This absorption justifies decrease in the C and N percentages and also increase in the H percentage of the experimental results. The elemental analysis on dry base was performed several times and the same percentages values were obtained for each experiment.[39] **"Table 1 Here"**

Thermal properties of the pure PBI and PBI/MoS_2 were studied by means of TGA at a heating rate of 20 °C/min under a nitrogen atmosphere. The PBI network exhibited remarkably high thermal stability. TGA data for PBI and all the PBI-MoS_2 with different percentage loadings of MoS_2 are shown in Fig. 4. All samples show weight loss at around 530-600 ^{o}C. These weight losses are due to the degradation of the polymer backbone. Table 2 summarizes the corresponding thermoanalysis data, including the temperatures at which 5% (T_5) as well as 10% (T_{10}) degradation occurs. Char yield is at 800 ºC and also limiting oxygen index (LOI) is based on Van Krevelen and Hoftyzer equation.[40]

$$LOI = 17.5 + 0.4\ CR$$

Where CR = char yield. From these data, it is clear that neat PBI and its NCs are stable at about 530 ºC, owing to the existence of heterocyclic benzimidazole ring. All samples had

LOI values higher than 40, calculated based on their char yield at 800 °C. On the basis of LOI values, such NCs can be classified as self-extinguishing materials. The obtained TGA data clearly indicates that the thermal stability of the PBI improved significantly after NCs formation with MoS_2 and the stability increased with increasing loading of MoS_2 nanoplates in PBI matrix. Interfacial interaction between PBI and MoS_2 has a very significant function in the thermal degradation of polymeric NCs. A suitable interfacial interaction permits MoS_2 nanoplates to act as a thermal barrier in the PBI matrix. The shielding ability depends on the dispersion patterns of the MoS_2 nanoplates in the polymer matrix. This aspect is related to both the nature and morphological features of the MoS_2 nanoplates in the PBI matrix. Since, in the current NCs, the morphological and structural feature changes with the MoS_2 loading (as seen in Fig. 4), we obtained a different level of thermal stability. This clearly proves the effect of morphologies in the thermal stability. In addition, as a typical layered inorganic material, MoS_2 is expected to disperse and exfoliate in the polymers and results in the physical barrier effects, which inhibit the diffusion of heat and the decomposition products of the polymer. Moreover, the transition metal element, Mo, promotes the formation of the charred layer acting as a physical barrier, which could slow down heat and mass transfer during the burning. So it is reasonable that MoS_2 may improve the thermal stability and fire resistance of polymer-based composites just like MMT, LDHs and grapheme.[26,41]

"Figure 4 and Table 2 Here"

The morphological information of MoS_2, PBI, and PBI-MoS_2 with 5 and 10% w/w of the MoS_2 characterized by FE-SEM are show in Fig. 5. According to the previous study,[6] in the MoS_2 nanoplate, Mo atoms are covalently bonded to S atoms in two adjacent S layers; the electroneutral MoS_2 slabs are held together by van der Waals interactions. Due to the weak interaction between the S-Mo-S layers, the slabs can be easily separated from each other, leading to a plate-like morphology with visible edges.[6] In this study, as shown in Figs. 5a and

5b, MoS_2 that obtained using L-cysteine in the layered structure, show plate-like morphology. In the other word, MoS_2 obtained through the proposed method consists of large-scale sheets that are tightly stacked together. Pure PBI shows two different types of morphology such as semi plate-like morphology and nanorod (Figs. 5, b and f). From these FE-SEM images (b and f), it is clearly observed that synthesized PBI is matrix with different distribution for morphology's elements. The obtained FE-SEM images, beside two different percent of PBI-MoS_2 (5 and 10 % w/w), are shown in Fig. 5 (c-h). According to these images in the PBI-MoS_2 hybrids, the micrograph exhibits a good dispersion of MoS_2 into polymer matrix. It seems that the particles are distributed uniformly in the polymer matrix with both of the plate-like and nanorod morphology. **"Figure 5 Here"**

The hybrid structure were further characterized using transmission electron microscopy (TEM) and TEM images of MoS_2 sheets beside PBI-MoS_2 (5% w/w) with two different magnifications are shown in Fig. 6. As shown in Figs. 6a and 6b, for MoS_2, the nanoparticles are actually in the form of irregularly sized nanopltate, and each MoS_2 nanosheet is well stacked to other plate-like MoS_2. On the other hand, in the case of PBI-MoS_2 (5% w/w), a mixture of PBI and MoS_2 nanosheets can be observed, in which the PBI simply serve as surface with uniform hole and MoS_2 nanosheets displays themselves by discrete connection. **"Figure 6 Here"**

XRD analysis of the synthesized samples (PBI, MoS_2, and PBI-MoS_2) is presented in Fig. 7. Figure 7 also shows XRD patterns of commercial MoS_2 and the synthesized MoS_2 nanoparticles. It appears that the commercial MoS_2 has strong crystallinity and a layered structure with an interlamellar distance of 6.15 Å (0.615 nm), as seen from the high order diffraction peaks (004), (006) and (008) as shown in Fig. 7. This highly crystalline material is very difficult to exfoliate and disperse in polymer matrices without special procedures However, MoS_2, synthesized by the above described method is unambiguously amorphous as

shown by the lack of crystalline or high-order basal peaks in the XRD diffractograms and is therefore presumably very dispersible in various polymer matrices. The absence of the (002) reflection at 6.15 Å ($2\theta=14.5^{o}$) and a broad feature indicating the absence of crystalline long-range order, strongly suggests a large extent of destacking in the synthesized MoS_2. Fig. 7 also shows the XRD pattern of PBI-MoS_2 NCs with 1% and 10 w/w of MoS_2 as compared to the MoS_2 and pure PBI. For neat PBI, several crystalline peaks were observed, indicating that this polymer is member of the crystal polymers. The XRD patterns of the PBI-MoS_2 NCs with 1% and 10 w/w of MoS_2 are characterized. AS shown in this figure, because of the low amounts of MoS_2, the peaks of amorphous MoS_2 could not be find. This complete disappearance of MoS_2 peaks may be due to the partial exfoliated structures.

"Figure 7 Here"

3.2. Electrochemical measurements

Electrochemical measurements were performed in a conventional three-electrode single cell at room temperature. A glassy carbon electrode (GCE) with a geometric surface area of 0.0314 cm^2 was used to prepare the modified working electrode. A Pt wire and Ag/AgCl were used as the counter and reference electrodes, respectively. Cyclic voltammograms (CVs) and liner sweep voltammetry (LSV) of the electrocatalysts were measured in a 0.5 M H_2SO_4 aqueous solution, to determine the hydrogen generation activity.

3.3 Electrocatalytic Activity of PBI and PBI-MoS_2

The catalytic activities of the PBI and PBI-MoS_2 with different percentage of MoS_2 (1%, 5%, and 10% w/w) for hydrogen generation were studied by electrochemical methods. The electrochemical activities of PBI and PBI-MoS_2, and MoS_2 were also studied and compared. Generally, an optimal hydrogen generation catalyst is a material that could give the highest current at the lowest overpotential, as well as a low hydrogen generation onset

potential (*i.e.*, the potential at which hydrogen generation activity begins) comparable to that of Pt catalyst. The Tafel slope, which can be deduced from Tafel equation ($\eta = b \log (j) + a$, where η is the overpotential, j is the current density and b is the Tafel slope), is always correlated with reaction pathway and the adsorption type.

First of all, the electrochemical activity of PBI was studied and compared with MoS_2 (Fig. 8A). The LSV curve of PBI shows an onset potential of –40 mV, while the curve of MoS_2 is more positive with a higher onset potential of about –60 mV. Moreover, PBI exhibits a current density of 10 mA cm^{-2} at overpotential of –40 mV, which is much smaller than MoS_2 (–8 mA cm^{-2} at –1.0 V). Possible reasons for different hydrogen generation activities of PBI and MoS_2 can be deduced from the morphological difference (TEM and FE-SEM) and hydrogen generation active sites. PBI has much more active sites (such as pyridinic-N and pyrrolic-N) than MoS_2 and according to the morphological analysis, PBI has several less aggregates than MoS_2, which cause the open structure for easy electron transfer. In this regard, PBI shows more uniform distribution of nanosheets and nanorods that exposed much more active edges, thus leading to the highest hydrogen generation catalytic activity.

In the second part, to developing new electrocatalyst for hydrogen generation, the electrocatalytic activity of the PBI-MoS_2 with different percentage of MoS_2 (1%, 5%, and 10% w/w) were investigated. In this regards, liner sweep voltammograms of the electrocatalysts were recorded in a 0.5 M H_2SO_4 aqueous solution, to determine the hydrogen generation activity. The results of LSV studied of PBI-MoS_2 (1%, 5%, and 10% w/w) catalysts are shown in Fig. 8B. As can be seen in the polarization curves, the different percentage of MoS_2 exhibits almost favorable hydrogen generation activity, particularly for 10% w/w PBI-MoS_2. However, when only 10% w/w of MoS_2 nanosheets is added to pure PBI, the onset potential of hybrid catalyst shifts to ~240 mV. Especially, upon the addition of 10% w/w of MoS_2, the overpotential value is close to ~160 mV. Thus, it demonstrates that

MoS_2 nanosheets are the core catalyst with abundant active edges for hydrogen generation, while MoS_2 sheets provide a conductive active sites and smaller sizes substrate affording more active edge sites for them. Moreover, with the further addition of MoS_2, the current density also is improved. **"Figure 8 Here".**

Undoubtedly, identifying the most active site(s) is critical to design and developed improved catalytic materials. In this study, electrocatalytic behaviors suggest that PBI has already carried an adequate load of active MoS_2 nanosheets. According to pervious study,[6] although bulk form of MoS_2 has a poor activity as a hydrogen generation catalyst, but nanoparticulate MoS_2 has high activity for this purpose. Due to achieving the excellent nanoparticulate properties of MoS_2 in PBI matrix, PBI-MoS_2 hybrid catalysts improved electronic contact between the active sites MoS_2 with PBI, thus exhibiting an enhanced their hydrogen generation activities. To clarify, PBI matrix contribute the MoS_2 sheets and nanoparticulates to reach their own exfoliated properties.

As an intrinsic properties of the electrocatalyst materials, the Tafel slopes, which is associated with the rate-limiting step of the hydrogen generation, have also been driven from the Tafel plots where their linear portions are fit well with the Tafel equations. For the PBI-MoS_2 10% w/w, the Tafel slope is 50.6 mV dec^{-1} which is better than for pure PBI (54 mV dec^{-1}). This is due to the fact that the conductivity of pure PBI is very small and it will be activated and increased its catalytic when the active sites and conductive sheets of MoS_2 incorporated with pure PBI's active edges. This result is well consistent with the polarization curves. When the dosage of MoS_2 nanosheets is increased to 10% w/w, as mentioned before, the Tafel slope shifts to 50.6 mV dec^{-1} which is comparable to the other MoS_2 catalysts. The hydrogen generation activities data for the proposed nanocomposites and for several recently reported electrocatalysts are compared in Table 3. **"Table 3 Here"**

3.4. Stability in the long-run

High durability was another important parameter for a good electrocatalyst. To assess the hydrogen generation stability of the catalysts, long-term potential cycling of PBI-MoS_2 10% w/w catalysts is better than the other synthetic electrocatalysts, when its tested in 0.5 M H_2SO_4 at room temperature by taking a potential scan at a scan rate of 20 mV/s, continuously for 1000 cycles. After the end of the cycles, not only any slight loss in the cathodic current was not observed for the PBI-MoS_2 10% w/w, but also the good stability of the catalysts and rising current density as well as reducing overpotentials was observed in acidic medium. In other words, the almost identical curve (Fig. 9) indicates high stability of PBI-MoS_2 10% w/w in a long-term electrochemical process. Hence these materials can be excellent electrocatalyst for hydrogen generation reaction. **"Figure 9 Here"**

3.5. Electrochemical impedance spectroscopy analysis

To understand the electrochemical behavior of the modified electrodes for hydrogen generation operating circumstance, electrochemical impedance spectroscopy (EIS) tests were conducted for pure PBI and PBI-MoS_2 hybrid (10% w/w). The Nyquist plots of PBI and PBI-MoS_2 hybrid measured at various negative potentials within the region corresponding to the LSV curves, as shown in Fig. 10. The best fitting was achieved using the Randles circuit (R_S, CPE and R_{ct}), and according to the solution resistance (R_S) in series with two parallel components, the charge-transfer resistance (R^{ct}) and a constant phase element (CPE), which is associated with the double layer capacitance. It can be seen that the sequence of the values of R_{ct} for the different modified-GCEs are as PBI-MoS_2 < PBI. **"Figure 10 Here"**

4. Conclusions

In summary, we synthesized a polycarboxyl aromatic monomers, 4,4',4"-((1,3,5-triazine-2,4,6-triyl)tris(azanediyl))tribenzoic acid, which was utilized to polymerize with 1,2,4,5-tetraaminobenzene to achieve a rich nitrogen polybenzimidazole network. The polycondensations could be completed in one-step within a short reaction time and at a

moderately low temperature, using a methane sulfonic acid-phosphorus pentoxide mixture as a medium. Their chemical structures were confirmed by FT-IR, ^{1}H NMR spectra, elemental analysis, and TGA. TGA results showed that PBI possess excellent thermal stability. Then, a series of organic/inorganic nanohybrid materials consisting of PBI with amorphous MoS_2 nanopalates are prepared by sonochemichal method. FT-IR, XRD, TEM, TGA, and FE-SEM experiments are carried out to characterize the morphologies and properties of the nanohybrids. Finally, the electrochemical behavior of the synthesized PBI and MoS_2 hybrids were evaluated for electrochemical hydrogen generation. By further MoS_2 in PBI matrix, the catalysts improved electronic contact between the active sites MoS_2 with PBI, thus exhibiting an enhanced their hydrogen generation activities. In this regards, the electrochemical studies showed that the obtained nanoelectrocatalys exhibited excellent hydrogen generation activities with an onset potential -160 mV *vs.* RHE. Large current densities, small Tafel slopes as well as prominent electrochemical durabilities are the main characteristic of these compounds. As the results, the newly proposed protocol opens a potential avenue for the development of high-performance Pt-free hydrogen generation catalysts.

Acknowledgements

We gratefully acknowledge the partial financial support from the Research Affairs division Isfahan University of Technology (IUT), Isfahan.

Reference:

1 M. G. Walter, E. L. Warren, J. R. McKone, S. W. Boettcher, Q. Mi, E. A. Santori and N. S. Lewis, *Chemical Reviews*, 2010, **110**, 6446–6473.

2 H. Bin Wu, B. Y. Xia, L. Yu, X.-Y. Yu and X. W. D. Lou, *Nature Communications*, 2015, **6**.

3 M. R. Singh, K. Papadantonakis, C. Xiang and N. S. Lewis, *Energy & Environmental Science*, 2015, **8**, 2760–2767.

4 J. a Turner, *Science (New York, N.Y.)*, 2004, **305**, 972–974.

5 N. S. Lewis and D. G. Nocera, *Proceedings of the National Academy of Sciences of the United States of America*, 2006, **103**, 15729–15735.

6 T. F. Jaramillo, K. P. Jørgensen, J. Bonde, J. H. Nielsen, S. Horch and I. Chorkendorff, *Science (New York, N.Y.)*, 2007, **317**, 100–102.

7 A. Le Goff, V. Artero, B. Jousselme, P. D. Tran, N. Guillet, R. Métayé, A. Fihri, S. Palacin and M. Fontecave, *Science (New York, N.Y.)*, 2009, **326**, 1384–1387.

8 P. D. Tran, A. Le Goff, J. Heidkamp, B. Jousselme, N. Guillet, S. Palacin, H. Dau, M. Fontecave and V. Artero, *Angewandte Chemie*, 2011, **123**, 1407–1410.

9 B. Winther-Jensen, K. Fraser, C. Ong, M. Forsyth and D. R. MacFarlane, *Advanced Materials*, 2010, **22**, 1727–1730.

10 F. A. Armstrong, N. A. Belsey, J. A. Cracknell, G. Goldet, A. Parkin, E. Reisner, K. A. Vincent and A. F. Wait, *Chemical Society Reviews*, 2009, **38**, 36–51.

11 X. Wang, K. Maeda, A. Thomas, K. Takanabe, G. Xin, J. M. Carlsson, K. Domen and M. Antonietti, *Nature materials*, 2009, **8**, 76–80.

12 T. Uchida, a Yamakata, Y. Sasaki and M. Osawa, *J. Am. Chem. Soc.*, 2009, **10862**, 10862.

13 Y. Zheng, Y. Jiao, Y. Zhu, L. H. Li, Y. Han, Y. Chen, A. Du, M. Jaroniec and S. Z. Qiao, *Nature Communications*, 2014, **5**, 3783.

14 H.-Y. Du, C.-H. Wang, C.-S. Yang, H.-C. Hsu, S.-T. Chang, H.-C. Huang, S.-W. Lai, J.-C. Chen, T. L. Yu and L.-C. Chen, *Journal of Materials Chemistry A*, 2014, **2**, 7015–7019.

15 E. Quartarone and P. Mustarelli, *Energy & Environmental Science*, 2012, **5**, 6436.

16 Y. Wang, Z. Shi, J. Fang, H. Xu, X. Ma and J. Yin, *Journal of Materials Chemistry*, 2011, **21**, 505.

17 S. Yang, X. Feng, X. Wang and K. Müllen, *Angewandte Chemie - International Edition*, 2011, **50**, 5339–5343.

18 C. V. Rao, C. R. Cabrera and Y. Ishikawa, *Journal of Physical Chemistry Letters*, 2010, **1**, 2622–2627.

19 M. Park, T. Lee and B.-S. Kim, *Nanoscale*, 2013, **5**, 12255–60.

20 Y.-C. Zhao, Q.-Y. Cheng, D. Zhou, T. Wang and B.-H. Han, *Journal of Materials Chemistry*, 2012, **22**, 11509.

21 M. G. Rabbani and H. M. El-Kaderi, *Chemistry of Materials*, 2012, **24**, 1511–1517.

22 H. Yu, M. Tian, C. Shen and Z. Wang, *Polymer Chemistry*, 2013, **4**, 961.

23 M. Dinari and H. Ahmadizadegan, *RSC Advances*, 2015, **5**, 8630–8639.

24 M. Dinari and P. Asadi, *RSC Advances*, 2015, **5**, 60745–60753.

25 Z. Guo, C. Yang, H. Wei, Y. Wang, J. Guo, L. Guan, X. Yan, X. Zhang and S. Wei, *Journal of Materials Chemistry A*, 2015.

26 K. Zhou, J. Liu, W. Zeng, Y. Hu and Z. Gui, *Composites Science and Technology*, 2015, **107**, 120–128.

27 J. Chen, N. Kuriyama, H. Yuan, H. T. Takeshita and T. Sakai, *Journal of the American Chemical Society*, 2001, **123**, 11813–11814.

28 X. Huang, Z. Zeng and H. Zhang, *Chemical Society Reviews*, 2013, **42**, 1934–1946.

29 K. Zhou, S. Jiang, C. Bao, L. Song, B. Wang, G. Tang, Y. Hu and Z. Gui, *RSC Advances*, 2012, **2**, 11695–11703.

30 Z. Matusinovic, R. Shukla, E. Manias, C. G. Hogshead and C. A. Wilkie, *Polymer Degradation and Stability*, 2012, **97**, 2481–2486.

31 L. Yang, S. Wang, J. Mao, J. Deng, Q. Gao, Y. Tang and O. G. Schmidt, *Advanced Materials*, 2013, **25**, 1180–1184.

32 K. Zhou, W. Yang, G. Tang, B. Wang, S. Jiang, Y. Hu and Z. Gui, *RSC Advances*, 2013, **3**, 25030–25040.

33 K. A Kolmakov, *Journal of Heterocyclic Chemistry*, 2008, **45**, 533–539.

34 K. Chang and W. Chen, *ACS nano*, 2011, **5**, 4720–4728.

35 P. E. Eaton, G. R. Carlson and J. T. Lee, *Journal of Organic Chemistry*, 1973, **38**, 4071–4073.

36 J. A. Asensio, S. Borrós and P. Gómez-Romero, *Journal of Polymer Science Part A: Polymer Chemistry*, 2002, **40**, 3703–3710.

37 P. Musto, F. E. Karasz and W. J. MacKnight, *Polymer*, 1993, **34**, 2934–2945.

38 H. Xu, K. Chen, X. Guo, J. Fang and J. Yin, *Polymer*, 2007, **48**, 5556–5564.

39 D. Ergun, Y. Devrim, N. Bac, I. Eroglu. J. Appl. Polym. Sci., 124: E267-E277, 2012

40 D.W. Van Krevelen and P.J. Hoftyzer, *Properties of polymers*, 3rd ed. Elsevier scientific publishing, New York, 1976.

41 S. Mallakpour, M. Dinari and A. Nabiyan, *Journal of Polymer Research*, 2015, **22**, 1-9.

42 Y Huang, Y. E. Miao, L. Zhang, W. W. Tjiu, J. Pan,. T. Liu, Nanoscale, 2014, **6**, 10673-10679.

43 S. Ji, Z. Yang, C. Zhang, Z. Liu, W. W. Tjiu, I. Y. Phang, Z. Zhang, J. Pan, T. Liu, Electrochim. Acta., 2013, **109**, 269-275

44 D. Y. Wang, M.Gong, H. L.Chou, C. J.Pan, H. A.Chen, Y. Wu, M. C. Lin, M.Guan, J. Yang, C. W.Chen, Y. L.Wang, B. J. Hwang, Ch. C.Chen, H. Dai, J. Am. Chem. Soc., 2015, **137**, 1587-1592.

45 H. Tang, K. P. Dou, C. C. Kaun, Q. Kuang, S. Yang, J. Mater. Chem. A, 2014, **2**, 360-364.

Table 1: The elemental analysis of the PBI

Elements	Theoretical	Experimental	Theoretical+16H_2O
C	65.6	48.90	48.64
N	30.6	21.10	22.69
H	3.6	5.30	5.62
O	0	24.7	23.04

Table 2: Thermal properties of the PBI and different PBI/MoS_2 hybrids.

Samples	Decomposition temperature (^oC)		Char yield (%)[b]	LOI[c]
	T_5 [a]	T_{10} [a]		
PBI	541	556	71	46
NC1%	566	576	73	46.7
NC5%	574	587	75	47.5
NC10%	581	600	77	48.0

[a] Temperature at which 5% and 10% weight loss was recorded by TGA at heating rate of 20 ^oC min^{-1} in an N_2 atmosphere.

[b] Weight percent of the material left undecomposed after TGA at maximum temperature 800 ^oC in an N_2 atmosphere.

[c] Limiting oxygen index (LOI) evaluated at char yield at 800 ^oC.

Table 3: Collected hydrogen activity data.

Catalyst	Overpotential (mV versus RHE)	Exchange current density ($mA\ cm^{-2}$)	Tafel slope ($mV\ decade^{-1}$)	Reference
MoS_2/SnO_2	-187	10	43	42
Exfoliated MoS_2	>-500	10	70	43
FeS_2/CNT	-120	20	46	44
$MoSe_2$/rGO	-115	10	69	45
PBI	-400	10	54	This work
PBI-MoS_2	~-160	10	50.6	This work

Legends for the Figures:

Fig. 1 Synthesis route to the TCA monomer and PBI networks.

Fig. 2 FT-IR of (a): 4,4',4''-((1,3,5-triazine-2,4,6-triyl)tris(azanediyl))tribenzoic acid (TCA), (b): neat PBI, (c): PBI-MoS_2 1%w/w, (d): PBI-MoS_2 5%w/w, (e): PBI-MoS_2 10%w/w and (f): pure MoS_2.

Fig. 3 ^1H NMR spectra of PBI. Numbers (1-26) indicate peaks arising from spinning side bands.

Fig. 4 TGA curves of PBI, PBI-MoS_2 1%w/w, PBI-MoS_2 5%w/w and PBI-MoS_2 10%w/w.

Fig. 5 FE-SEM images of (a and e): MoS_2, (b and f): PBI**,**(c and g): PBI-MoS_2 5%w/w, (d and h): PBI-MoS_2 10%w/w.

Fig. 6 TEM images of (a and b): MoS_2 sheets and (c and d): PBI-MoS_2 (5% w/w)**.**

Fig.7 XRD pattern of: Commercial MoS_2, MoS_2 Synthesized, PBI, PBI-MoS_2 1% w/w, and PBI-MoS_2 10% w/w.

Fig. 8 Linear sweep voltammograms for hydrogen evaluation reaction in 0.5 mol L^{-1} H_2SO_4 at (A): (a): PBI, (b): amorphous MoS_2, (B): Linear sweep voltammograms for hydrogen evaluation reaction in 0.5 mol L–1 H_2SO_4 at (a): PBI-MoS_2 10% w/w, (b): PBI-MoS_2 5% ,and w/w, (c): PBI-MoS_2 1% w/w.

Fig. 9 Linear sweep voltammograms for long-term electrochemical stability test of PBI-MoS_2 10%w/w in 0.5 mol L^{-1} H_2SO_4 at (A): 1th, 200th, 400th, 600th, 800th, 1000th cycles, with a scan rate of 20 mV s^{-1}**.**

Fig. 10 Nyquist plots (from electrochemical impedance spectroscopy data) at (A): PBI modified GCE in different potential *vs.* Ag/AgCl. Conditions: electrolyte, 0.5 mol L^{-1} H_2SO_4. B): Nyquist plots of PBI-MoS_2 (10%w/w) modified GCE in different potential *vs.* Ag/AgCl. Conditions: electrolyte, 0.5 mol L^{-1} H_2SO_4.

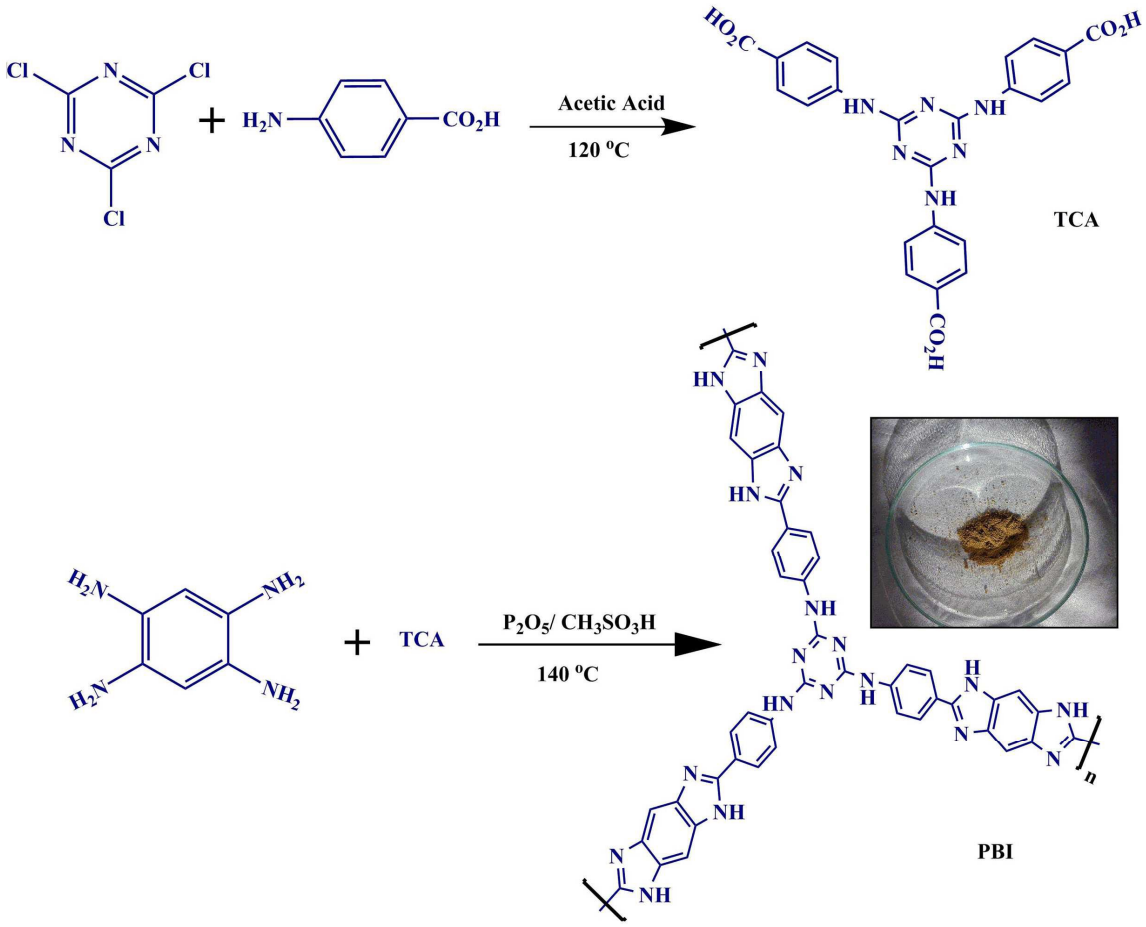

Fig. 1

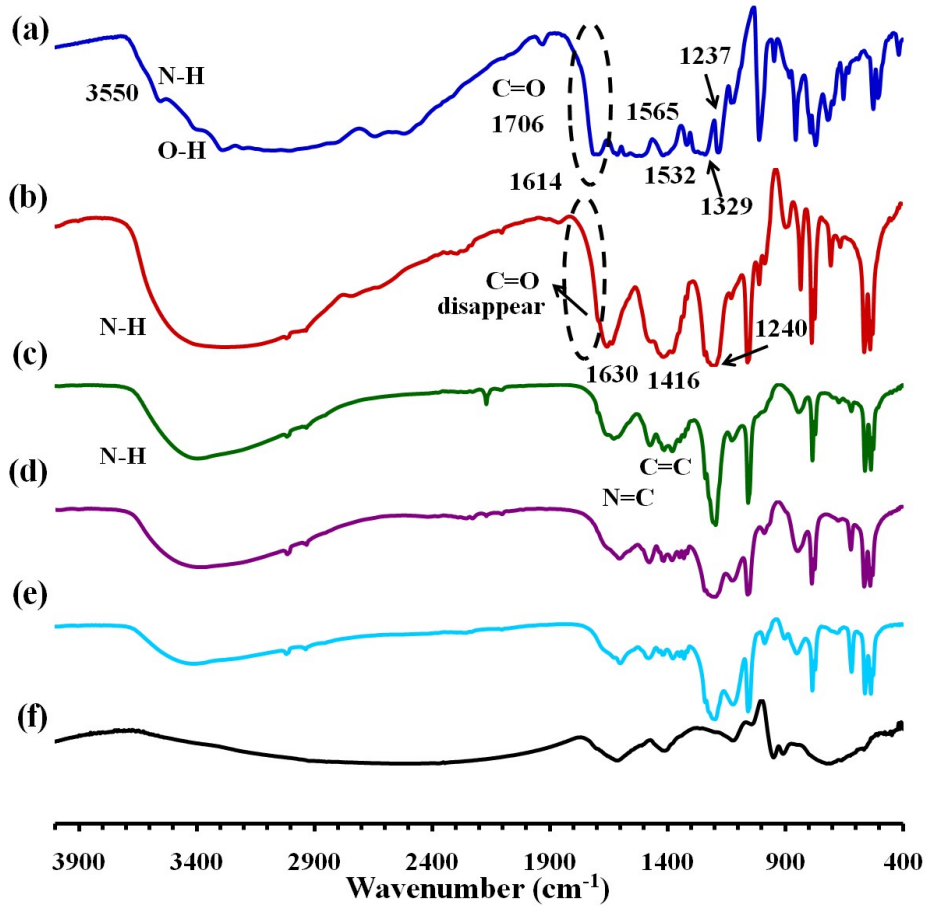

Fig. 2

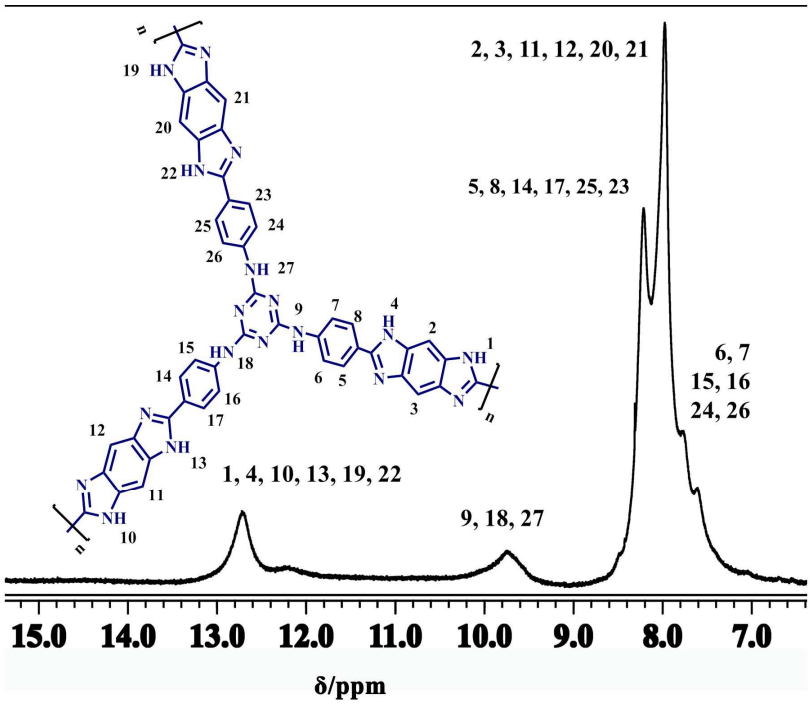

Fig. 3

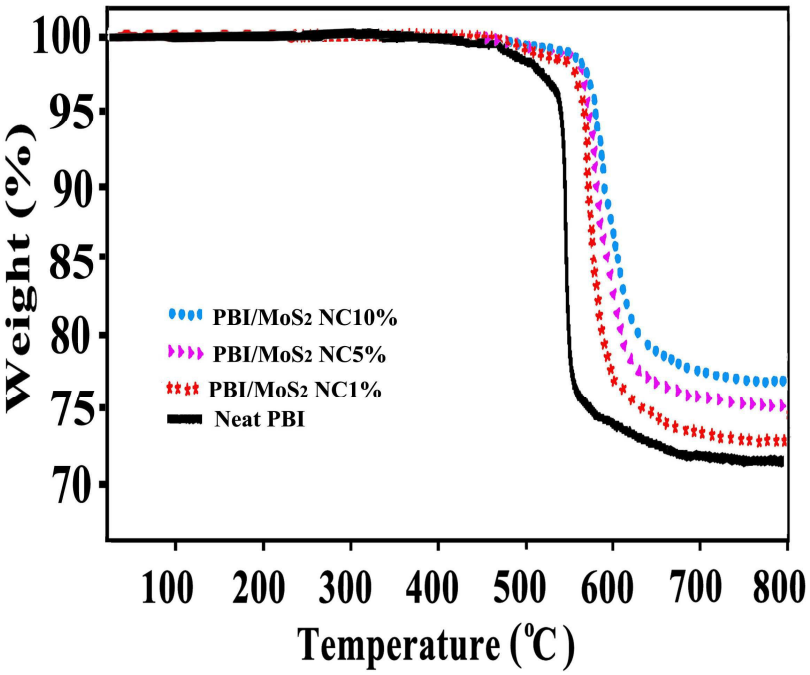

Fig. 4

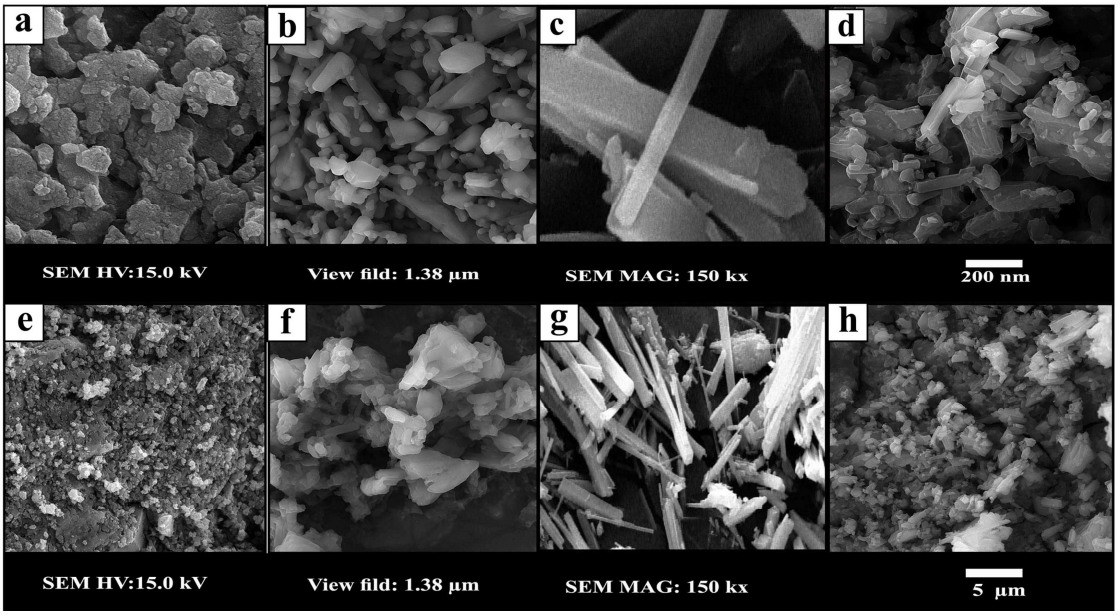

Fig. 5

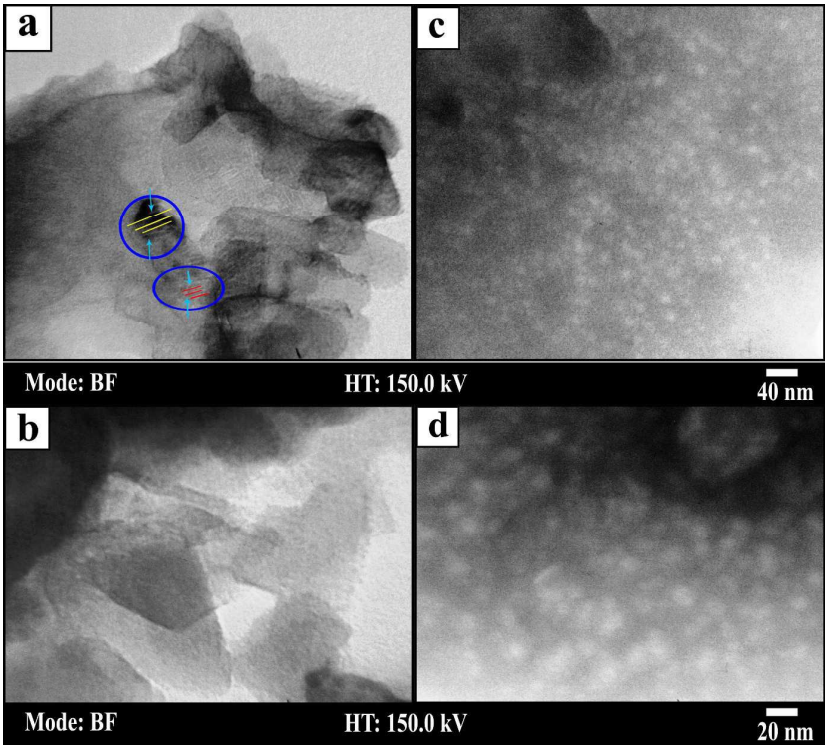

Fig. 6

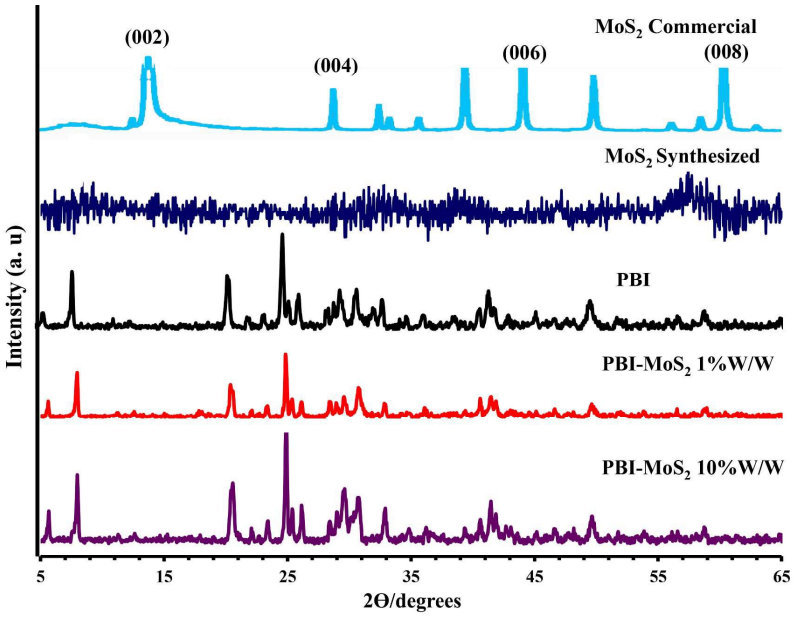

Fig.7

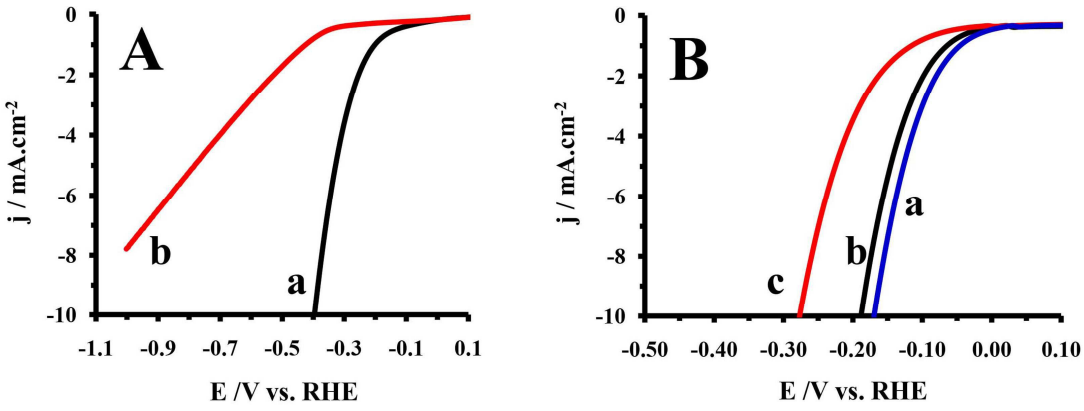

Fig. 8

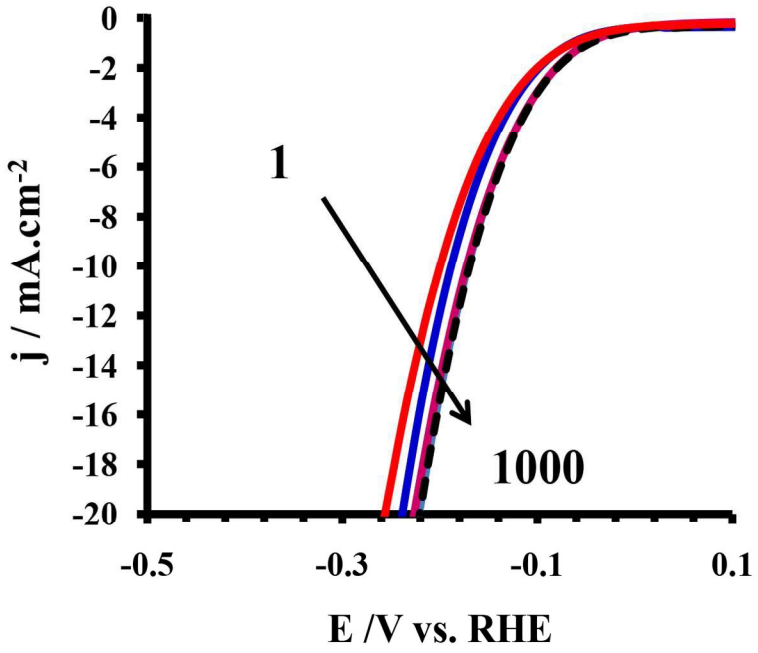

Fig. 9

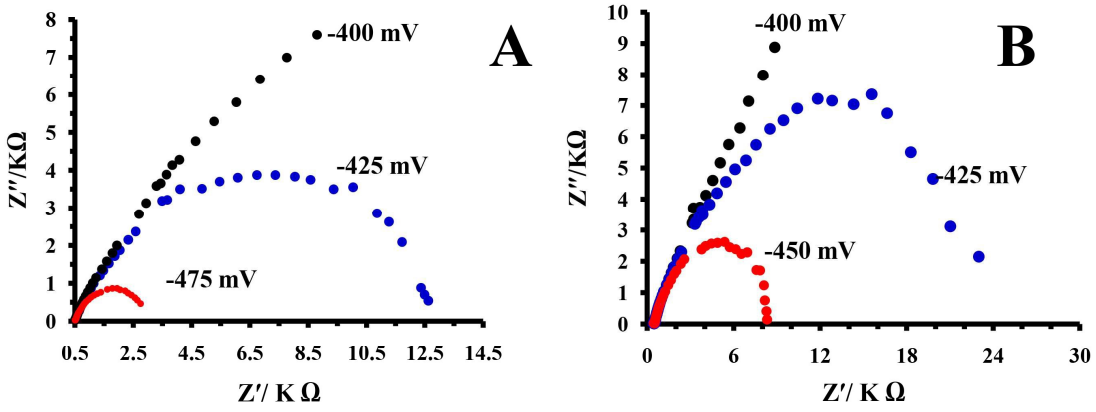

Fig. 10

Graphical Abstract with text

High active nitrogen site polybenzimidazole network was synthesized through polycondensation and it was modified with amorphous MoS_2 for hydrogen generation.